Analysis of Envelope-Tracking Power Amplifier Using Mathematical Modeling

Jooseung Kim, *Student Member, IEEE*, Dongsu Kim, Yunsung Cho, *Student Member, IEEE*, Daehyun Kang, Byungjoon Park, Kyunghoon Moon, *Student Member, IEEE*, and Bumman Kim, *Fellow, IEEE*

***Abstract*—This paper describes analysis of an envelope-tracking power amplifier (ET PA) to show its operational behavior. The RF PA is modeled by sweeping the input power and supply voltage. The RF PA model is composed of three 2-D lookup tables including the amplitude-to-amplitude modulation, amplitude-to-phase modulation, and amplitude-to-efficiency modulation. The hybrid switching supply modulator is also modeled using an ideal op-amp, ideal switches, and other assisting blocks. Based on the mathematical models of the RF PA and supply modulator, the ET PA can be analyzed with a fast calculation speed and a good accuracy to find the optimum ET operation point. A power control strategy is presented for the optimal ET operation over a broad output power range. The effect of the delay mismatch on the characteristics of the ET PA is also described to assist the time alignment algorithm. For a 10-MHz long-term evolution signal with a 7.44-dB PAPR, the implemented ET PA at 1.71 GHz delivers a PAE of 44.3%, a gain of 29 dB, an evolved universal terrestrial radio access adjacent channel leakage ratio of −35.1 dBc, and an error vector magnitude of 2.91% at an average output power of 28 dBm.**

***Index Terms*—Envelope tracking (ET), long-term evolution (LTE), power amplifier (PA), supply modulator.**

I. Introduction

RECENT wireless communication systems use spectrally efficient complex modulation schemes to achieve high data throughput within limited spectrum resources. The fourth-generation (4G) systems require using a modulation, which generates a high peak-to-average power ratio (PAPR) and wide channel bandwidth (BW) signal. Unfortunately, efficiency of the conventional fixed supply RF power amplifier (RF PA) is low when the amplifier is operated under these conditions [1]. Especially, the RF PAs for the high-end mobile handsets should be efficient, while supporting the complex 4G signals, to reduce the heat and to increase the battery lifetime. Therefore, many power-saving techniques have been studied for a long time [2]–[20].

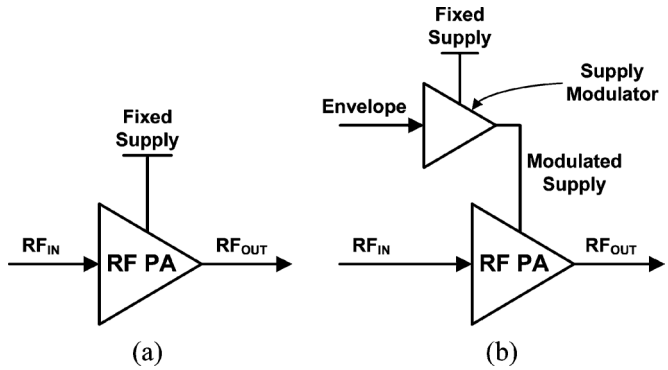

Fig. 1. (a) Conventional PA with fixed supply voltage. (b) ET PA with modulated supply voltage.

Until recently, an average power tracking (APT) technique is applied to real systems to improve efficiency of the RF PA at the back-off power region. In the APT system, dc supply of the RF PA is adjusted according to the average RF power. A dc–dc converter for the APT operation is simple and has a high efficiency across a broad output power range [2]. The APT PA works fine when the PAPR of the signal is relatively small such as second-generation (2G) and third-generation (3G) systems. However, the dissipated power of the RF PA is very high for 4G signals, and it will be more serious in the future systems because of the increased PAPR.

An envelope-tracking (ET) technique is one of the favorable candidates to solve this problem. Although ET system is more complex than the APT system and requires use of more sophisticated supply modulator, it can improve efficiency of the RF PA for amplification of the modulated RF signal with a high PAPR. Fig. 1(a) and (b) shows simplified block diagrams of a conventional PA and an envelope-tracking power amplifier (ET PA), respectively. By replacing the fixed supply with the dynamic supply voltage, the dc power consumption of the ET PA is reduced compared to that of the conventional PA, and the efficiency is significantly increased, as shown in Fig. 2. Since the supply voltage of the RF PA is modulated by the supply modulator, the overall efficiency of the ET PA is proportional to the efficiency of the supply modulator. Therefore, the supply modulator should be optimally designed to have a high efficiency without generating significant distortion. To achieve high efficiency and wideband operation, the supply modulator has been researched based on the hybrid switching structure,

Manuscript received November 18, 2013; revised February 03, 2014; accepted April 24, 2014. Date of publication May 09, 2014; date of current version June 02, 2014. This work was supported by the Ministry of Science, ICT and Future Planning (MSIP), Korea of the ICT R&D Program 2013.

J. Kim and K. Moon are with the Department of Electrical Engineering, Pohang University of Science and Technology (POSTECH), Pohang, Gyeongbuk 790-784, Korea.

D. Kim is with Samsung Electronics, Suwon-si, Gyeonggi 443-742, Korea.

Y. Cho and B. Park are with the Division of IT Convergence Engineering, Pohang University of Science and Technology (POSTECH), Pohang, Gyeongbuk 790-784, Korea.

D. Kang is with the Broadcom Corporation, Matawan, NJ 07747 USA.

B. Kim is with the Department of Electrical Engineering, Pohang University of Science and Technology (POSTECH), Pohang, Gyeongbuk 790-784, Korea, and also with the Division of IT Convergence Engineering, Pohang University of Science and Technology (POSTECH), Pohang, Gyeongbuk 790-784, Korea.

Color versions of one or more of the figures in this paper are available online at http://ieeexplore.ieee.org.

Digital Object Identifier 10.1109/TMTT.2014.2321356

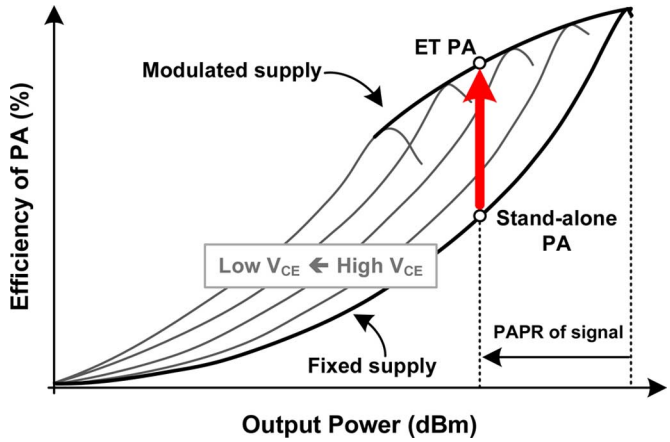

Fig. 2. PA's efficiency curves with fixed and modulated supply voltages.

which is composed of a linear regulator and a switching mode power supply (SMPS) [3]–[18]. To enhance efficiency of the supply modulator, a feed-forward signal, a dual-switch, and a multi-phase pulsewidth modulation (PWM) control are studied in [3]–[5]. This research results in a highly efficient SMPS, which supplies a large amount of current to the load and determines the overall efficiency of the supply modulator. For a high-speed operation, BW of the linear regulator is improved in [6], enabling accurate tracking of the wideband signal without generating distortions. For applying to the real system where the supply is directly connected to a battery, a boost-mode hybrid switching supply modulator is introduced in [8], forming a power management integrated circuit (PMIC). Furthermore, the ET PA can be also operated for a multimode system by properly designing the modulator [10]. These efforts lead to a point where the ET technique is applied to mobile devices.

For further improvement of the ET PA, the RF PA and supply modulator should be optimized, and research on interlocking of the RF PA and supply modulator is also essential. Even if the same RF PA and supply modulator are interlocked to implement an ET PA, the ET PA delivers different characteristics such as efficiency, gain, linearity, AM–AM, and AM–PM depending on the interlocking. In this study, we analyze the characteristics of the ET PA to find an optimum ET operating point. We also present the effect of the delay mismatch on those characteristics and describe a power control strategy of the ET PA for the optimal operation over the entire average output power range.

This paper is organized as follows. Section II describes the mathematical modeling and the performance of the RF PA with several dc supplies. Section III details the characteristics of the ET PA based on the models, the effect of the delay mismatch, and the power control strategy of the ET PA. Section IV presents the measured results and the conclusions are discussed in Section V.

II. Mathematical Modeling of ET PA

A. Mathematical Model

Fig. 3 shows a mathematical modeling of the ET PA, which includes models of the PA and the supply modulator. An entire simulation environment is depicted in Fig. 3(a). The output data of digital $\mathrm{I_{OUT}}$, $\mathrm{Q_{OUT}}$, and efficiencies (η_{SM}, η_{PA}, η_{ET}) can be calculated from the input data of digital I and Q. It consists of a PA model, a supply modulator model, a Cartesian-to-polar converter, a polar-to-Cartesian converter, a delay block, an envelope shaping block, and a variable gain amplifier (VGA). The VGA is used to sweep the input power of the RF PA in the simulation environment. Since all signals are operated only in baseband domain, not in RF frequency, and the models are simple mathematical models rather than a complex transistor based model, it calculates at a fast speed with a good accuracy. The used modulation signal is a long-term evolution (LTE) with 10-MHz channel BW, 7.44-dB PAPR, and 16-QAM modulation scheme. The time duration and sampling rate of this simulation are 0.5–1 ms and 2×61.44–32×61.44 MS/s, respectively, and these values can be adjusted for accuracy or speed.

Fig. 3(b) shows the PA model, which is composed of three 2-D lookup tables (LUTs) for amplitude-to-amplitude modulation (AM–AM), amplitude-to-phase modulation (AM–PM), and amplitude-to-efficiency modulation (AM–EM). The LUTs are generated from a harmonic balance (HB) simulation of the designed PA by sweeping its input power and supply voltage, but memory effects are not included in this model. The modeled PA has a two-stage configuration using the HBT process, and input and output are matched to an operating frequency of 1.85 GHz. The output harmonic load is tuned as a class-AB/F type [22]. The inputs of the LUTs are input amplitude ($\mathrm{A_{IN}}$) and supply voltage ($\mathrm{V_{DD.PA}}$). The output amplitude ($\mathrm{A_{OUT}}$) is generated using a 2-D interpolation ($\mathrm{f_{AMAM}(A_{IN}, V_{DD.PA})}$) of the AM–AM LUT. The output phase (θ_{OUT}) is equal to a sum of the input phase (θ_{IN}) and a phase modulation ($\mathrm{f_{AMPM}(A_{IN}, V_{DD.PA})}$) from the AM–PM LUT. The AM–EM LUT is necessary to calculate the efficiencies (η_{SM}, η_{PA}, η_{ET}) and the current ($\mathrm{I_{PA}}$) flowing from the supply modulator to the PA. The PA model can analyze the intermodulation distortion (IMD) behavior of the RF PA [23] and characterize the linearity sweet spot evolution in the device [24]. The PA model in this study is focused on the operational characteristics of the ET PA according to the input power and supply voltage to analyze the interconnection behavior between the supply modulator and RF PA.

Fig. 3(c) shows a model of the hybrid switching supply modulator. The model consists of an ideal op-amp, an inductor with a dc resistance (DCR), ideal switches with ON resistances, a hysteretic comparator, and other assisting blocks. In the model, the ideal op-amp and ideal switches with ON resistance are the linear regulator and switching converter of the real hybrid switching supply modulator, respectively. Although the model does not use real transistors and does not include distortions from the op-amp and the switching converter, its operation and efficiency are almost the same with the supply modulator based on the real transistors. The input envelope voltage ($\mathrm{V_{ENV}}$), which is the same with the output envelope voltage ($\mathrm{V_{DD.PA}}$), is detected from the input data of the digital I and Q, and is reshaped by the envelope shaping block. The supply current ($\mathrm{I_{PA}}$) is determined by the AM–EM LUT. The efficiency of the supply modulator can be expressed as

$$\eta_{\mathrm{SM}} = \frac{P_{\mathrm{OUT.SM}}}{P_{\mathrm{DC.SM}}} \tag{1}$$

$$P_{\mathrm{OUT.SM}} = \overline{V_{\mathrm{DD.PA}} \cdot I_{\mathrm{PA}}} \tag{2}$$

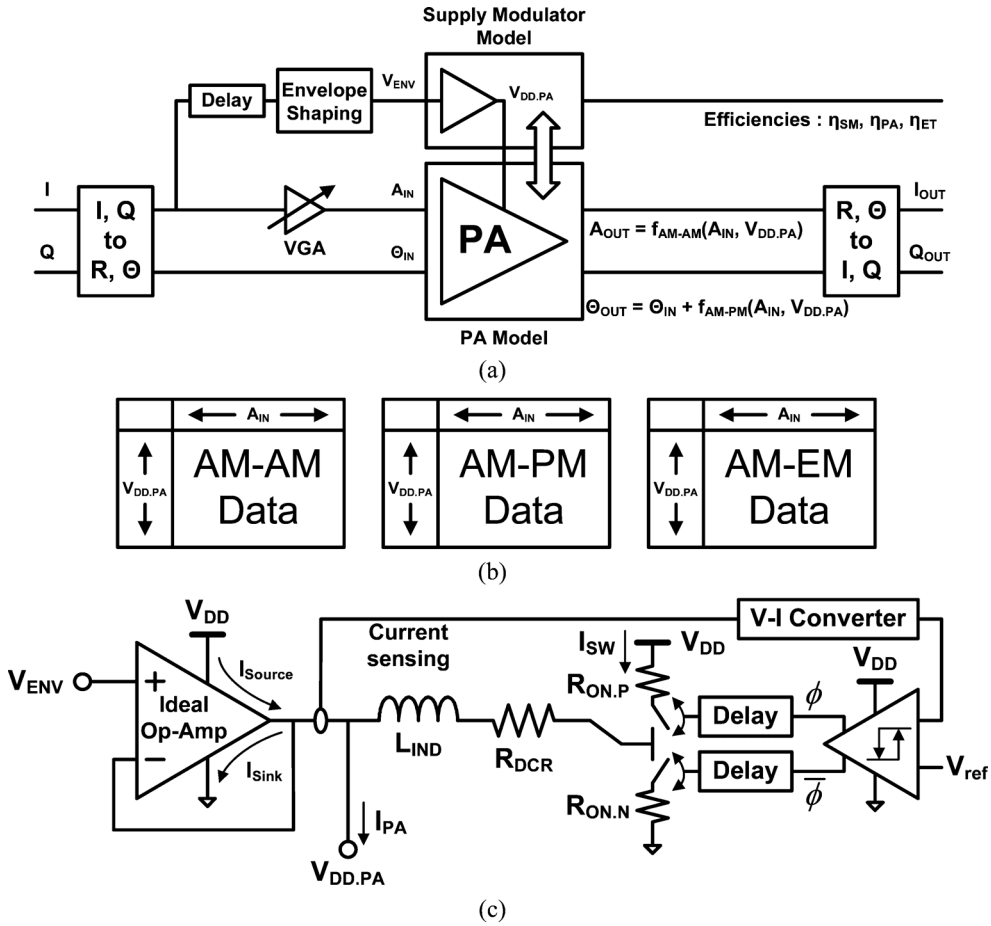

Fig. 3. Mathematical modeling of ET PA. (a) Entire simulation environment. (b) 2-D LUTs for PA model. (c) Model of hybrid switching supply modulator.

$$P_{\mathrm{DC.SM}} = V_{\mathrm{DD}} \cdot \left(\overline{I_{\mathrm{Source}}} + \overline{I_{\mathrm{SW}}} + I_{\mathrm{Static}} + f_{\mathrm{SW.AVG}} \cdot Q_{\mathrm{SW.Driver}} \right) \quad (3)$$

where $\mathrm{P_{OUT.SM}}$ and $\mathrm{P_{DC.SM}}$ are the output power and power consumption of the supply modulator, respectively. $\mathrm{I_{Source}}$ and $\mathrm{I_{SW}}$ are the dissipated currents in the op-amp and the switching converter, respectively. $\mathrm{I_{Static}}$ includes the static currents in an OTA, a class-AB biasing circuit, a current sensor, a V-I converter, and a hysteretic comparator. $\mathrm{f_{SW.AVG}} \cdot Q_{\mathrm{SW.Driver}}$ is a current to present the switching loss in the switching converter. The switching loss is proportional to the average switching frequency $(\mathrm{f_{SW.AVG}})$ and the $\mathrm{Q_{SW.Driver}}$ is a MOSFET input charge for driving the switching converter. Generally, $\mathrm{f_{SW.AVG}}$ is dependent on the hysteresis value, inductance, and some other parameters for a narrowband signal. For a wideband signal, $\mathrm{f_{SW.AVG}}$ is mainly determined by the signal BW. Based on these mathematical models of the PA and supply modulator, we analyze the characteristics of the ET PA to find the optimum ET operation condition.

B. Performance of PA at Each DC Supply

Fig. 4 shows the simulated continuous wave (CW) performances of the PA with several dc supplies. The dc supply is swept from 0.5 to 4.5 V. The 0.5 V is a minimum supply voltage to prevent the operation below the knee voltage, and the 4.5 V is a maximum supply voltage for a reliable operation of the modeled HBT PA. As the dc supply decreases, the maximum output power of the PA is reduced, and the influence of the knee voltage becomes larger, lowering the drain efficiency (DE). The equivalent load resistance $(\mathrm{R_{PA}})$ can be expressed as $\mathrm{V_{DD.PA}}/\mathrm{I_{PA}}$. Therefore, $\mathrm{R_{PA}}$ increases as the output power decreases because $\mathrm{I_{PA}}$ is reduced with a constant $\mathrm{V_{DD.PA}}$. At the same output power, $\mathrm{R_{PA}}$ is lower with the reduced $\mathrm{V_{DD.PA}}$. However, for the real ET operation, $\mathrm{V_{DD.PA}}$ and $\mathrm{I_{PA}}$ dynamically follow the power level, and $\mathrm{R_{PA}}$ is almost constant. The gain of the fixed supply PA is flat across the broad output power range. On the other hand, the gain of the dynamic supply PA gradually increases as the dc supply rises due to the increased maximum available gain (MAG) of the transistor. The deep class-AB biased PA also has a gain expansion characteristic as introduced in [23], but the reason of the gain expansion is different with the ET PA. Therefore, the linearity of the ET PA according to the average input power is quite different from the standalone PA.

III. Characteristics of ET PA

A. Linearity of ET PA

To analyze linearity of the ET PA and find its optimum operating point, the ET PA and standalone PA are simulated. The simulation is based on the mathematical models, and its setup is shown in Fig. 5. The ET PA has a modulated supply voltage

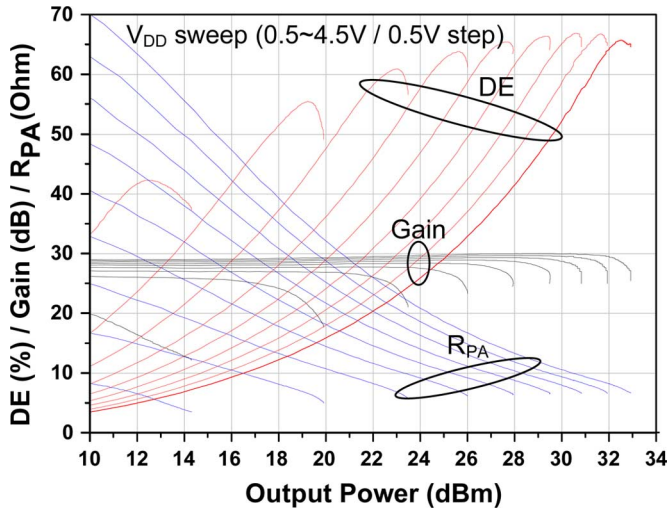

Fig. 4. Simulated CW performances of RF PA by sweeping the collector voltage from 0.5 to 4.5 V.

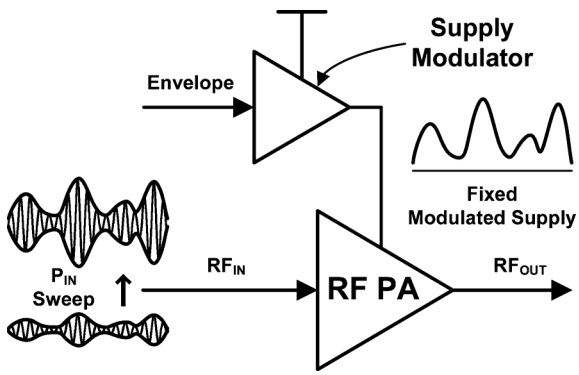

Fig. 5. Simulation setup of ET PA for fixed modulated supply.

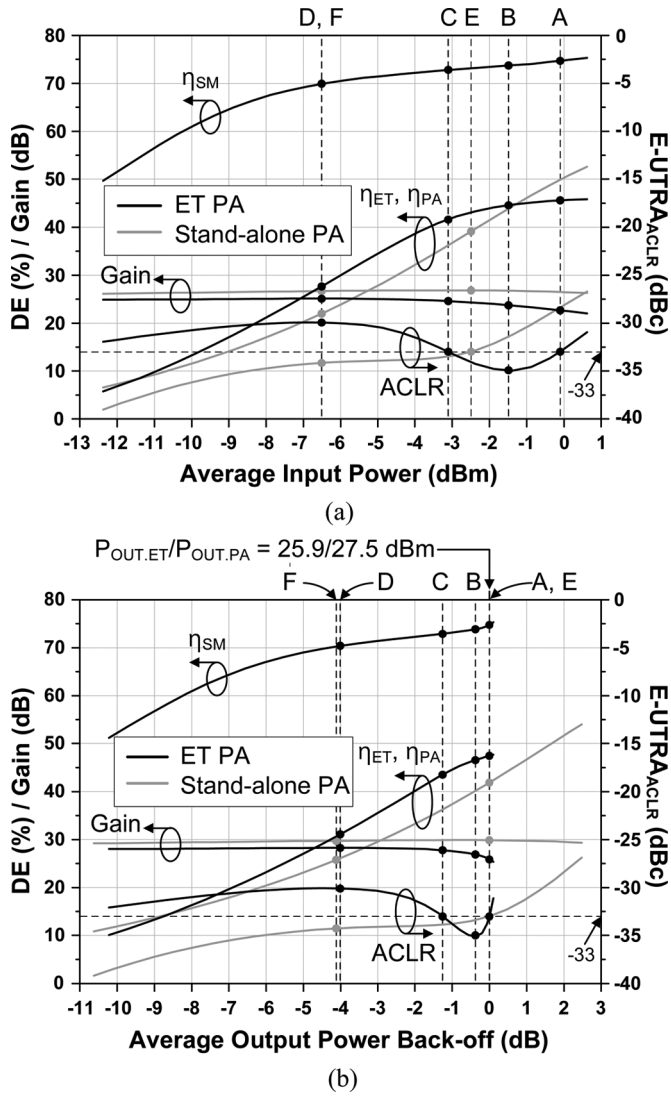

Fig. 6. Simulated performances of ET PA and standalone PA for fixed modulated supply according to: (a) average input power and (b) average output power back-off level.

with the fixed voltage swing range of 0.5–4.5 V, and the standalone PA has a fixed supply of 4.5 V. The input powers of both PAs are swept from -12.4 to 0.6 dBm with the fixed supplies. The linearity of the ET PA can be estimated according to the input power for a fixed envelope, and compared with that of the standalone PA. Fig. 6(a) and (b) shows the simulated results of the ET PA and standalone PA for a 10-MHz LTE signal with a PAPR of 7.44 dB, which illustrate the performances over the average input power and power back-off level from the peak average output power, respectively. The peak average output powers for the two PAs are defined for the maximum power level at E-UTRA$_{\mathrm{ACLR}}$ of -33 dBc. The standalone PA has a higher gain and a larger saturated output power than the ET PA, as shown in Fig. 6(b) because of the larger effective drain bias. The DEs of the both PAs increase as the average input power rises [see Fig. 6(a)], and the ET PA has a higher efficiency at the peak power level compared to that of the standalone PA [see Fig. 6(b)] although its power is lower. For a more detailed analysis, the six points indicated in Fig. 6 are analyzed; the points A–D and E–F correspond to the ET PA and standalone PA, respectively. Generally, the linearity of the standalone PA is degraded as the average input power is raised because the PA is pushed into saturation region $(\mathrm{F} \rightarrow \mathrm{E})$. On the other hand, the ET PA has a different linearity characteristic. For the fixed modulated supply, the linearity at a low average input power operation such as the D point is poor due to the large gain expansion, as shown in Fig. 4. However, the linearity of the ET PA is gradually improved up to the point B when the average input power is raised, and gets worse after that forming a sweet spot at point B. When this average input power is applied, the PA is saturated, but the distortion is properly compensated by the gain expansion characteristic of the ET PA. Fig. 7 shows the instantaneous curves of the DE, gain, and $\mathrm{R_{PA}}$ for the ET PA (A, B, C, D) and standalone PA (E, F). These curves are overlaid on the curves in Fig. 4. For the operation at point C, the PA is operated in the saturation region, but the gain compression is not enough to compensate the gain expansion characteristic of the ET PA. On the other hand, the ET PA operation at point A is rather heavily saturated, and it has a gain compression characteristic. The gain curve of the ET PA at point B is flattest,

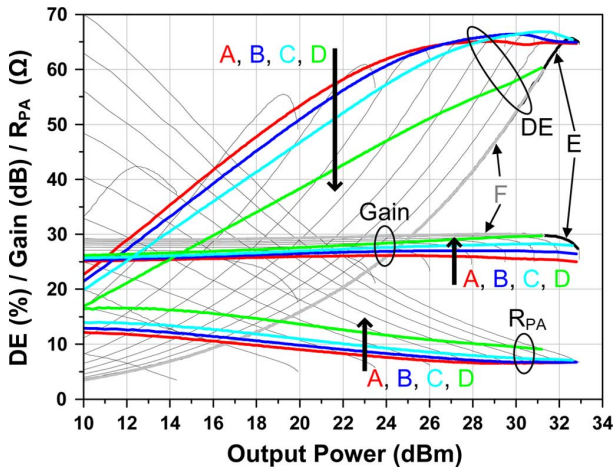

Fig. 7. Instantaneous operation curves of DE, gain, R_{PA} for ET PA (A, B, C, D) and standalone PA (E, F) overlaid on the drain bias dependent responses.

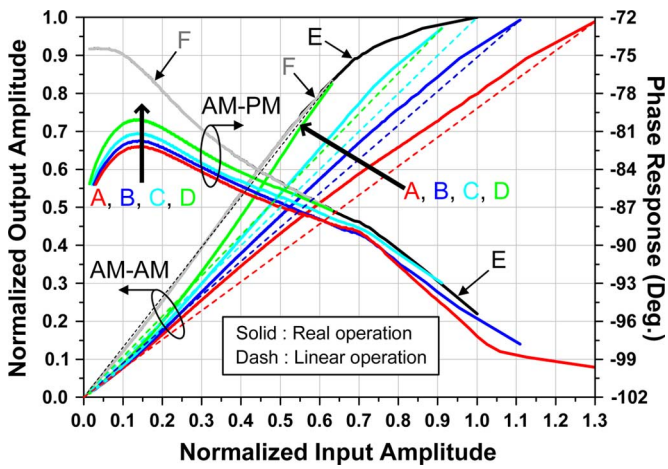

Fig. 8. AM–AM and AM–PM curves of ET PA (A, B, C, D) and standalone PA (E, F).

providing the best linearity. At the same E-UTRA$_{ACLR}$ condition, the DE of the ET PA is a lot higher than that of the standalone PA, and it is highest at point A operation. The R_{PA} of the ET PA is decreased as the average output power is raised (D → A). The linearity is also analyzed from the AM–AM and AM–PM curves for the ET PA and standalone PA, as depicted in Fig. 8. The AM–AM response has a similar tendency with the gain characteristic in Fig. 7. The standalone PA is linearly operated at a low input power, but is abruptly saturated. For the ET PA, the output power at the low input power region is larger than the linear output power due to the gain expansion, but the difference is gradually reduced because the ET PA is operated in the saturation region. The AM–AM curve at the point B operation is the most linear. The AM–PM characteristic is affected by the input and output capacitances of the PA, but the output capacitance is generally the dominant one. The phase response of the modeled PA in this paper has a decreasing AM–PM characteristic as the input power increases. The phase variation of the ET PA is smaller than that of the standalone PA. To analyze the AM–PM characteristic of the ET PA, the output capacitance

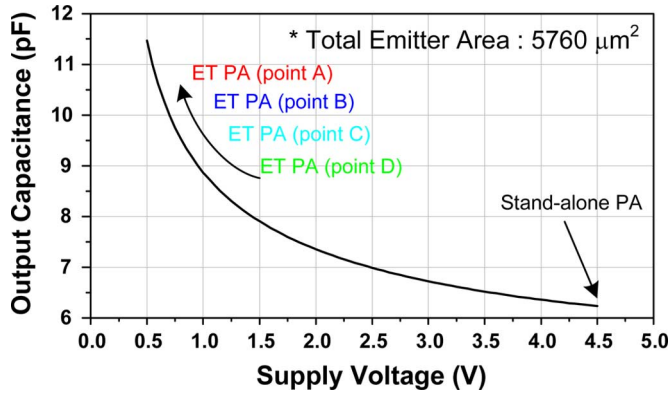

Fig. 9. Output capacitance of the PA at a fixed input power according to the supply voltage.

TABLE I
PERFORMANCE SUMMARY OF ET PA AND STANDALONE PA USING MATHEMATICAL MODEL

	ET PA				Stand-alone PA	
	A	B	C	D	E	F
P_{OUT} (dBm)	25.9	25.5	24.6	21.9	27.5	23.4
Gain (dB)	25.9	26.9	27.8	28.2	29.9	29.7
η_{ETPA} (%)	47.5	46.5	43.5	31.2	41.9	25.7
DE_{PA} (%)	63.5	63.1	59.7	44.3		
η_{SM} (%)	74.8	73.8	72.9	70.4	-	-
E-UTRA$_{ACLR}$ (dBc)	-33.0	-35.1	-33.0	-30.1	-33.0	-34.3

is plotted by sweeping the supply voltage at a fixed input amplitude, as shown in Fig. 9 [21]. The output capacitance is inversely proportional to the supply voltage. The supply voltage of the ET PA is dynamically reduced at a lower input power region, and it is further lowered from point D to point A when the input amplitude is the same. Therefore, the output capacitance is the highest at point A and the lowest at point D among the ET PA at the same input amplitude. On the other hand, the supply voltage of the standalone PA is fixed to 4.5 V regardless of the input amplitude, and the output capacitance can not be larger than that of the ET PA. The increased output capacitance of the ET PA causes the decreased phase response at the low input power region compared to the standalone PA.

Although point A operation has a higher efficiency than point B, the linearity is best at point B. To optimally compensate the gain expansion characteristic of the ET PA, a proper average input power should be applied to the PA. The efficiency and linearity of the ET PA are in tradeoff relation depending on the average input power. The simulated results of the ET PA (A, B, C, D) and the standalone PA (E, F) are summarized in Table I.

B. Effect of Delay Mismatch in ET PA

The previous analyses are carried out under the assumption that the time alignment between the RF and envelope signals is

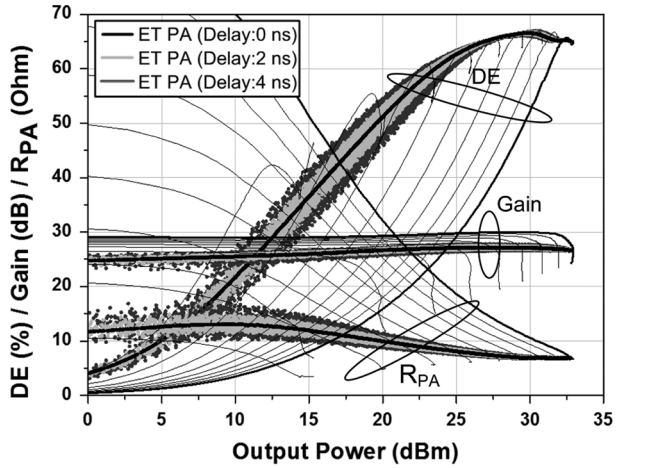

(a)

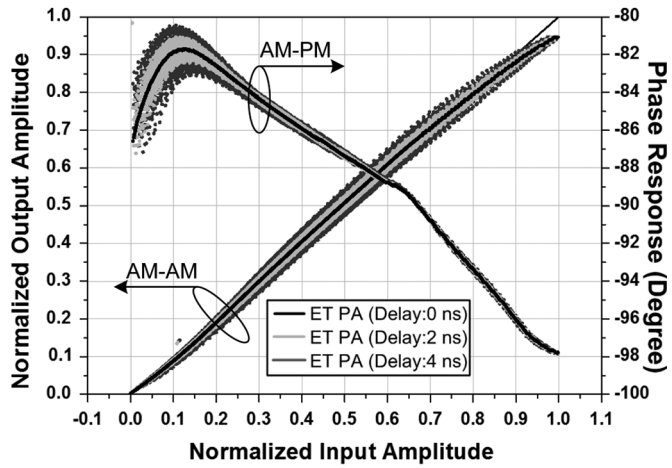

(b)

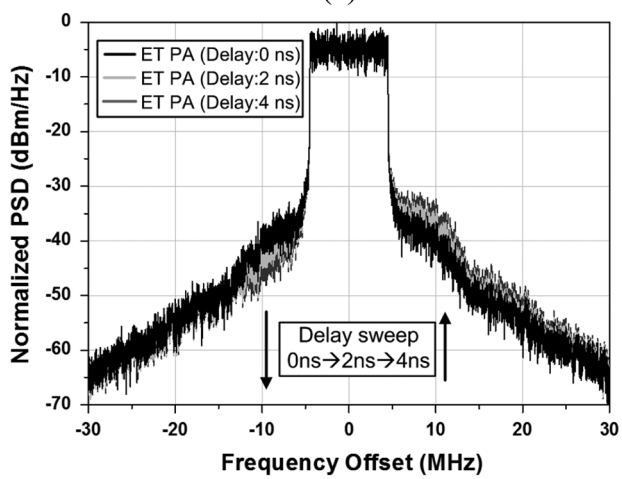

(c)

Fig. 10. Characteristic of ET PA according to the envelope delay. (a) DE, gain, and equivalent load resistance. (b) AM–AM and AM–PM. (c) Power spectrum density.

perfectly matched. In this section, we analyze the effect of the delay mismatch in the ET system.

To test the delay mismatch, the envelope signal is artificially aligned with positive and negative delays, while the RF signal is fixed. Fig. 10 shows the simulated results according to the envelope delays. When the time alignment is not matched, an improper supply voltage is instantaneously applied to the PA and the different output power is generated. Therefore, the DE, gain, $\mathrm{R_{PA}}$, AM–AM, and AM–PM characteristics are dispersed as shown in Fig. 10(a) and (b). The dispersion is similar to the memory effect of the PA, and it causes the asymmetric power spectrum as depicted in Fig. 10(c). The positive delay of the envelope results in the increment on the right side and the decrement on the left side of the spectrum. For the fixed modulated supply, the efficiency of the supply modulator, DE, output power, and $\mathrm{E\text{-}UTRA_{ACLR}}$ are simulated according to the delay mismatch to analyze the sensitivity. Fig. 11 shows those values for the ET operations at points A, B, and C. The efficiency of the supply modulator, DE, and output power of the ET PA are insensitive to the delay mismatch, while $\mathrm{E\text{-}UTRA_{ACLR}}$ significantly varies according to the delay mismatch. When the positively delayed envelope signal is applied to the supply of the PA, the upper $\mathrm{E\text{-}UTRA_{ACLR}}$ is degraded and the lower $\mathrm{E\text{-}UTRA_{ACLR}}$ is improved. The negative delay of the envelope signal causes the opposite $\mathrm{E\text{-}UTRA_{ACLR}}$ characteristic. Among the points A, B, and C, the linearity at the point B operation is rather sensitive to the delay mismatch, but the upper and lower $\mathrm{E\text{-}UTRA_{ACLR}}$'s are lowest up to the 5-ns mismatch.

To analyze the output spectrum variation for the delay mismatch according to the AM–PM characteristic of a PA, the PA having an increasing AM–PM characteristic, which is reverse to our modeled AM–PM characteristic, is evaluated. In this case, the positive delay of the envelope results in the decrement on the right side and the increment on the left side of the spectrum, and the negative delay is vice versa. This variation is opposite to the result of the PA having the decreasing AM–PM characteristic, as depicted in Fig. 12. Therefore, if the AM–PM characteristic of the PA is known, we can determine the positive or negative delay mismatch from the output spectrum. This technique can be useful for the time alignment algorithm.

C. Power Control Strategy of ET PA

The DE, gain, linearity, AM–AM, and AM–PM characteristic of the ET PA are analyzed at a certain average output power in the previous sections. In this section, we present a power control strategy for the optimal ET operation over a broad average output power. By applying a proper shaped envelope signal to the supply of the PA for the given output power level, the ET PA can deliver a high efficiency and good linearity simultaneously [12].

Fig. 13 shows the η_{SM}, $\mathrm{DE_{PA}}$, $\mathrm{DE_{ETPA}}$, gain, and $\mathrm{E\text{-}UTRA_{ACLR}}$ according to the average output power with several back-off envelope signals. The best linearity points, which are the sweet spots (point B) in different magnitudes of the envelope signal, are traced, and the other characteristics are also traced based on those points. Although the $\mathrm{DE_{ETPA}}$'s are not maximum values for the shaping, they are not significantly different from the peak efficiency. To track the best linearity points, the envelope signal should be scaled following the shaping function represented in Fig. 14. The envelope signal is shaped from 0.5 to 4.5 V, considering the knee voltage of the HBT PA and the voltage drop of the linear regulator. Beyond 4.5 V, the envelope signal is clipped. It is possible to achieve a

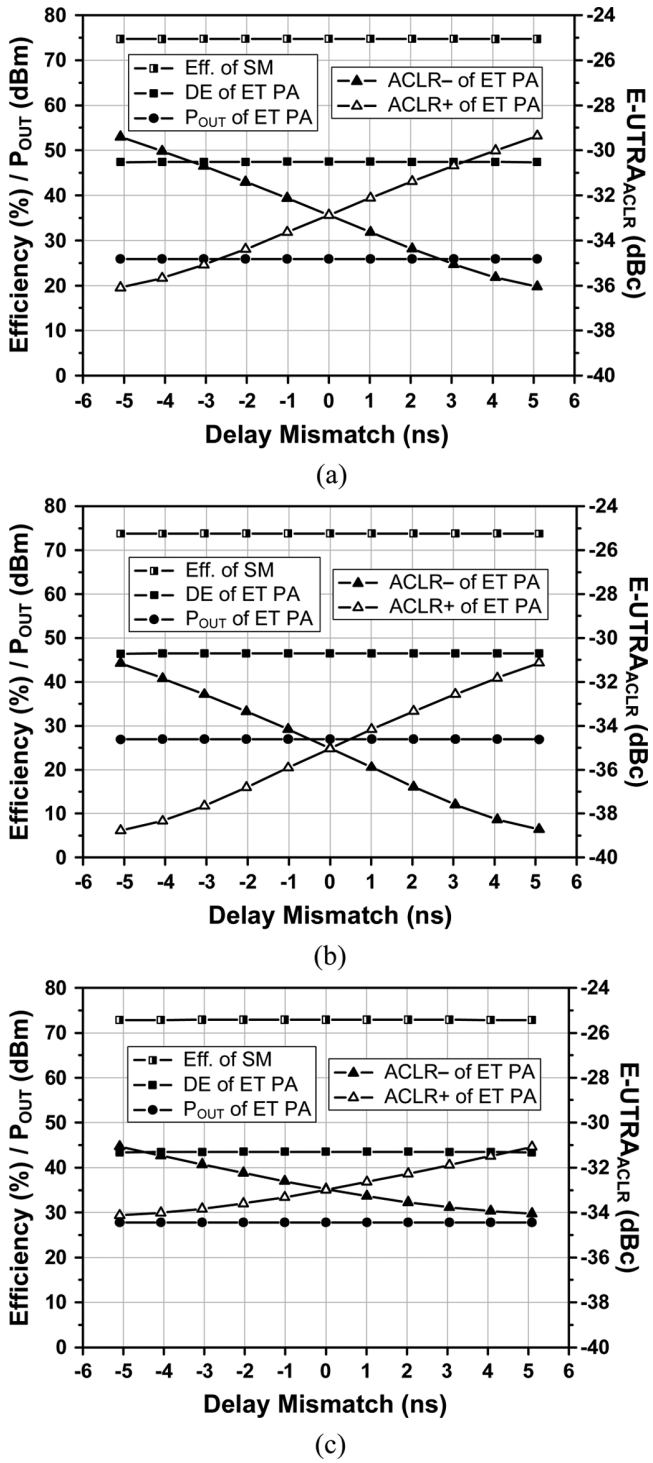

Fig. 11. Efficiency of supply modulator, DE, output power, and E-UTRA$_{\mathrm{ACLR}}$ of the ET PA according to delay mismatch. (a) Point A. (b) Point B. (c) Point C.

high power and high efficiency by clipping the envelope signal with a heavy driving of RF signal, and is similar to the crest factor reduction (CFR) technique to reduce the PAPR [25], [26].

IV. Measurement Results

The implemented ET PA is composed of a supply modulator and a class-AB PA. The PA is fabricated using an InGaP/GaAs HBT process and its operating frequency is 1.71 GHz. The supply modulator is fabricated using a 0.18-μm CMOS process and it uses thick oxide I/O devices for a high-voltage operation. Chip photographs of the designed supply modulator and PA are shown in Fig. 15, and their sizes are 1.35 mm $\times$ 1.35 mm and 1.2 mm $\times$ 1.0 mm, respectively. The supply voltage of the ET PA is 5 V and the envelope swing range is from 0.5 to 4.5 V.

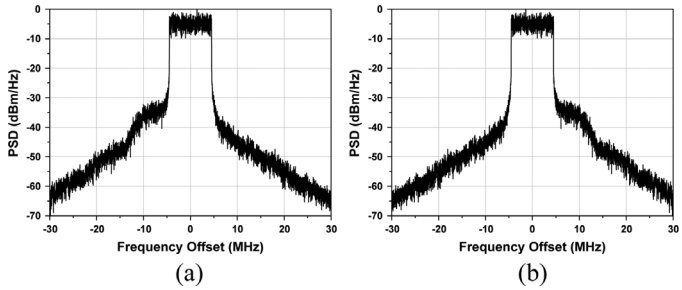

Fig. 12. Output power spectrum density of ET PA according to positive/negative delay and decreasing/increasing AM–PM. (a) Decreasing AM–PM with negative delay or increasing AM–PM with positive delay. (b) Decreasing AM–PM with positive delay or increasing AM–PM with negative delay.

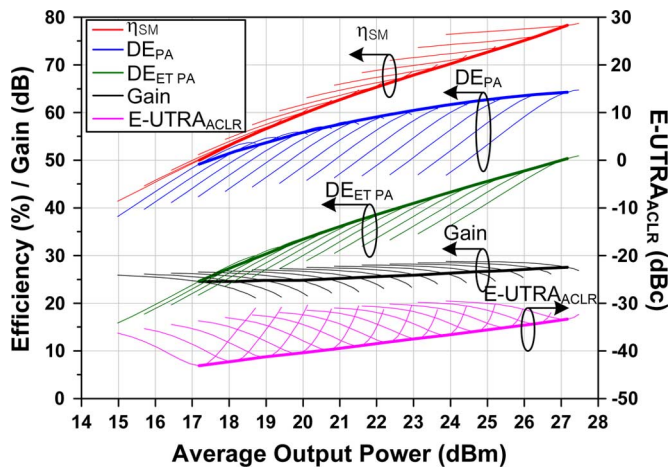

Fig. 13. η_{SM}, $\mathrm{DE}_{\mathrm{PA}}$, $\mathrm{DE}_{\mathrm{ETPA}}$, gain, and E-UTRA$_{\mathrm{ACLR}}$ according to average output power with several magnitudes of modulated supply.

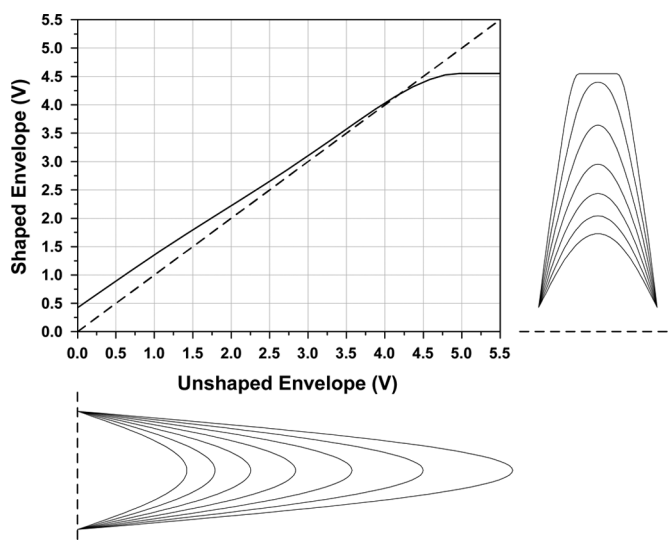

Fig. 14. Proposed envelope shaping function.

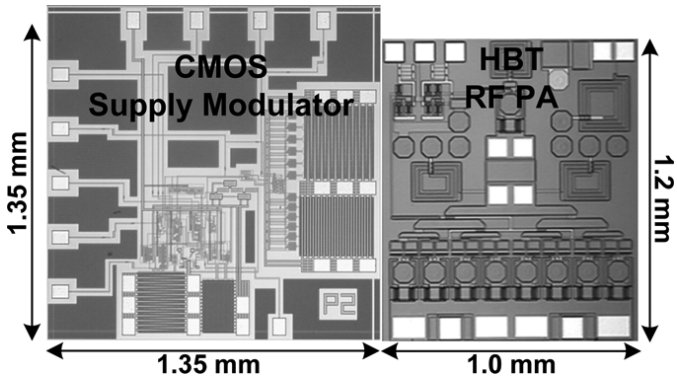

Fig. 15. Chip microphotographs of the supply modulator and the RF PA.

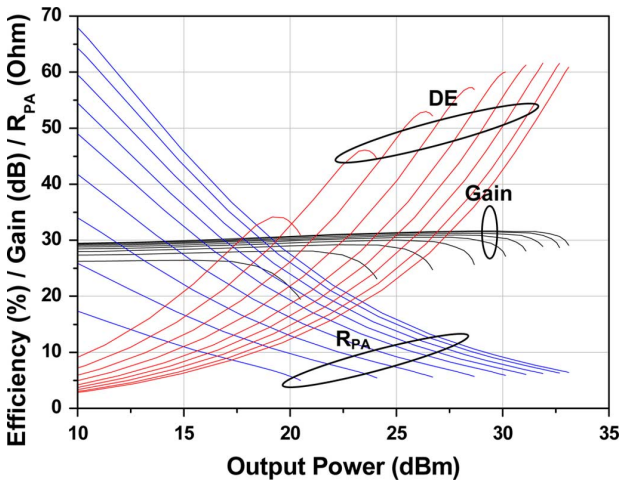

Fig. 16. Measured CW performances of RF PA by sweeping the collector voltage.

To test the supply modulator, the PA is modeled as a 6.5-Ω resistive load. For the 16-QAM LTE envelope signal with 10-MHz signal BW and 7.44-dB PAPR, the supply modulator delivers a measured efficiency of 75.3%. The PA has a two-stage configuration for a high gain. It delivers a P1 dB of 32.6 dBm, gain of 30.6 dB, and PAE of 58.1% with the supply voltage of 4.5 V. Fig. 16 shows the measured CW performances of the PA by sweeping the supply voltage.

To implement the ET PA at the optimum operating point, the ET PA is measured by sweeping the average input power for the fixed modulated supply, and compared to the standalone PA whose supply is fixed to 4.5 V (see Fig. 17). The ET PA has a higher PAE than the standalone PA by reducing the dc power consumption. When the average output power is raised, the linearity of the ET PA is improved up to a certain power point and gets worse above the level, which is similar to the simulation results. Fig. 18 shows the measured performance of the ET PA according to the delay mismatch between the RF and envelope signals. To test and measure the effect of the delay mismatch, the envelope and RF signals are generated using two synchronized signal generator, which can control the positive/negative delay of envelope or RF signal. The PAE and gain of the ET PA are maintained regardless of the delay mismatch, while $\mathrm{E\text{-}UTRA_{ACLR}}$ is sensitive, as shown in Fig. 18(a). The sensitivity of the linearity according to the

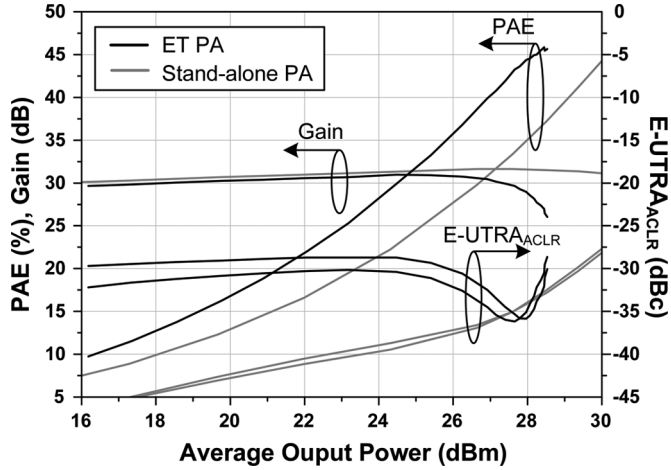

Fig. 17. Measured performances of the standalone PA and ET PA with the fixed modulated supply according to the average output power.

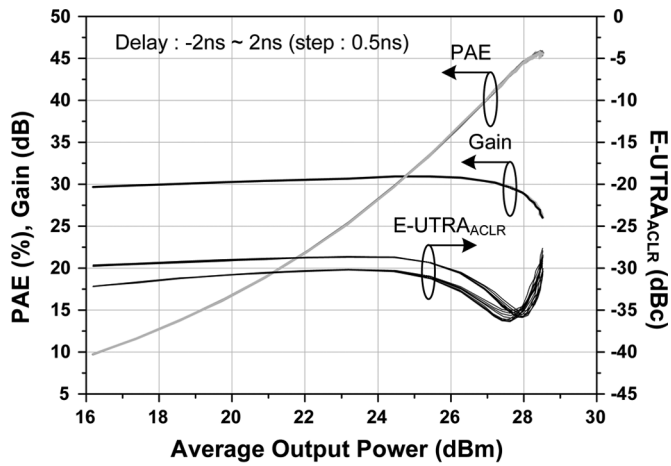

(a)

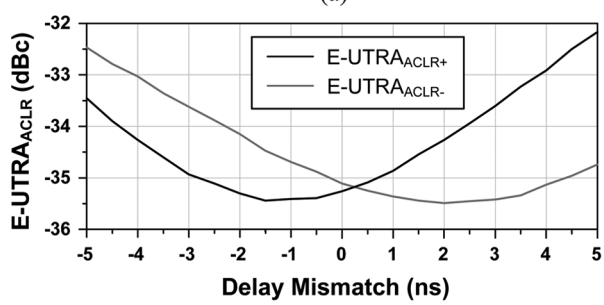

(b)

Fig. 18. (a) Measured performance of ET PA with fixed modulated supply according to average output power with several envelope delays. (b) $\mathrm{E\text{-}UTRA_{ACLR}}$ according to the delay mismatch.

delay mismatch is represented in Fig. 18(b). The measured upper and lower $\mathrm{E\text{-}UTRA_{ACLR}}$'s are similar to the simulated results up to ±2-ns delay, but they are degraded after that due to the slightly different characteristic of the PA with the simulated one. The ET PA does not have a dc decoupling capacitor ($\sim\mu$F) at the supply line of the RF PA to inject the envelope signal, while the supply line of the RF PA in the simulation is an ideal one with the dc decoupling capacitor. The linearity of the ET PA according to the delay mismatch is also illustrated

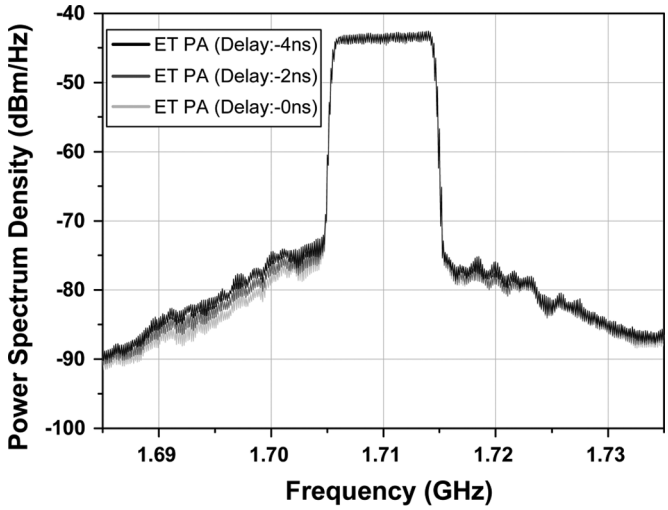

(a)

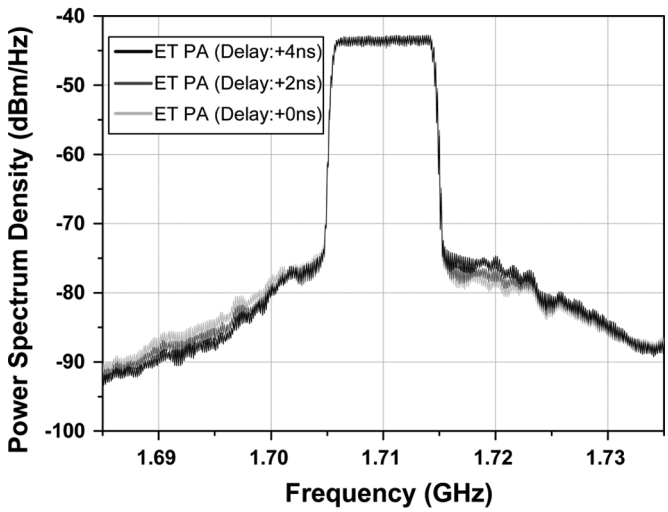

(b)

Fig. 19. Measured spectra of ET PA with: (a) negative envelope delays and (b) positive envelope delays.

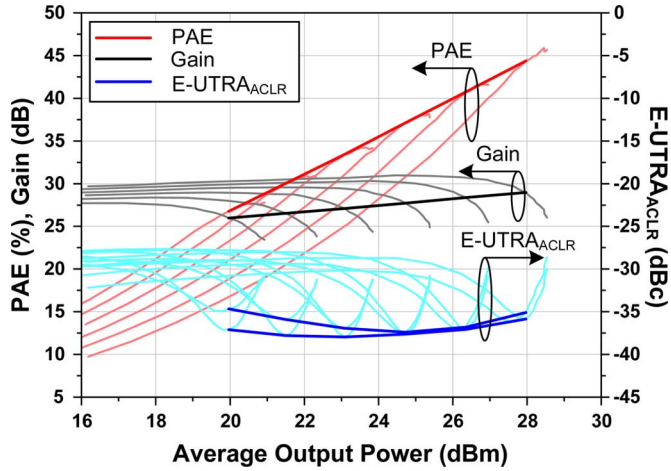

Fig. 20. Measured performance of ET PA according to average output power with several magnitudes of modulated supplies.

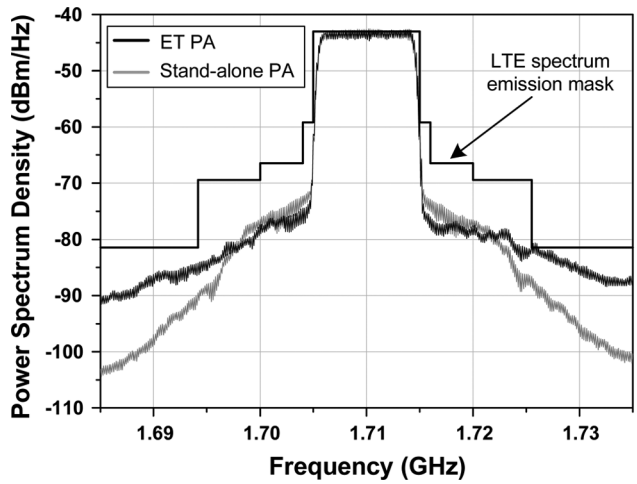

Fig. 21. Measured spectra of the ET PA and standalone PA at the maximum average output power with spectrum emission mask for 10-MHz LTE signal.

in Fig. 19. The delay mismatch causes the asymmetric power spectrum. Since the measured PA has a decreasing AM–PM characteristic as the input power increases, the positive delay results in the increment on the right side of the spectrum and the negative delay results in the increment on the left side of the spectrum.

The PAE, gain, and E-UTRA$_{\mathrm{ACLR}}$ of the ET PA are measured according to the average output power with several magnitudes of the modulated supply, as shown in Fig. 20. The best E-UTRA$_{\mathrm{ACLR}}$ points are traced, and the PAE and gain are also traced based on those points. The measured performance has a similar tendency with the simulated results. Based on the measured results, we can say that the ET PA can be operated in the optimum points over the broad output power region, and achieve a high efficiency and good linearity simultaneously. At an average output power of 28 dBm, the ET PA delivers a PAE of 44.3%, a gain of 29 dB, an E-UTRA$_{\mathrm{ACLR}}$ of -35.1 dBc, and an EVM of 2.91%. The output spectra of the ET PA and standalone PA are plotted in Fig. 21. The spectra satisfy the 10-MHz LTE spectrum emission mask at the maximum average output power. The measured performances of the ET PA based on the analyses in this paper are summarized together with the recent state-of-art results in Table II.

V. Conclusion

An ET PA is analyzed using mathematical models of the RF PA and supply modulator to find an optimum ET operating point for a high efficiency and good linearity simultaneously. The RF PA model is composed of three LUTs for AM–AM, AM–PM, and AM–EM by sweeping the input power and supply voltage, while the supply modulator is modeled using an ideal op-amp, ideal switches, and other assisting blocks. From the simulation using the models, we have found that the ET PA also creates a sweet spot and the envelope should be shaped following the spot. In this shaping, the ET PA delivers the best linearity with the DE similar to the maximum value. The output spectra of the ET PA are also analyzed according to the delay mismatch between the RF and envelope signals. The mismatch creates a spectrum response similar to the memory effect. According to the leading or lagging mismatch and decreasing or increasing AM–PM characteristic, the one side of the spectrum

TABLE II
PERFORMANCE COMPARISON WITH STATE-OF-THE-ART RESULTS

Ref.	Application	Signal BW (MHz)	PAPR (dB)	Freq. (GHz)	η_{SM}* (%)	Pout (dBm)	Gain (dB)	PAE (%)	EVM‡ (%)	Technology
[7]	LTE 16-QAM	10	-	1.9	-	23.4	15†	38	4.9	0.35-μm SiGe BiCMOS
[8]	LTE 16-QAM	10	-	2.535	76.8	25.8	24.8	32.3	2.8†	0.35-μm CMOS, HBT
[11]	LTE 16-QAM	10	7.44	1.85	77.5	28.9	24.5†	42.2	2.69	0.18μm CMOS, HBT
[15]§	LTE	20	6.6	2.535	70.5	29	28.5	43	$<$1.9	0.15μm CMOS, GaAs HBT
[17]	LTE 16-QAM	10	7.5	1.85	75	26	-	34.1	2.8	0.18μm CMOS
[19]	LTE	10	-	0.707	-	27.5	32	37.1	-	InGaP HBT
This work	LTE 16-QAM	10	7.44	1.71	75.3	28	29.0	44.3	2.91	0.18-μm CMOS, HBT

*SM : Supply Modulator †graphically estimated ‡LTE specifications : EVM $<$ 12.5% §With DPD linearization

increases and the other side decreases. This information can be useful for the time-alignment algorithm. A power control strategy is also described for the optimal ET operation over the broad output power range. Through the ET PA operation at the optimal condition, we achieve a highly linear and efficient PA. For a 10-MHz LTE signal with a 7.44-dB PAPR, the implemented ET PA at 1.71-GHz delivers a PAE of 44.3%, gain of 29 dB, E-$\mathrm{UTRA}_{\mathrm{ACLR}}$ of -35.1 dBc, and EVM of 2.91% at an average output power of 28 dBm.

REFERENCES

[1] M. K. Kazimierczuk, *RF Power Amplifiers*. New York, NY, USA: Wiley, 2008.

[2] A. Tombak, D. C. Dening, M. S. Carroll, J. Costa, and E. Spears, "High-efficiency cellular power amplifiers based on a modified LDMOS process on bulk silicon and silicon-on-insulator substrates with integrated power management circuitry," *IEEE Trans. Microw. Theory Techn.*, vol. 60, no. 6, pp. 1862–1869, Jun. 2012.

[3] T. Kwak, M. Lee, and G. Cho, "A 2 W CMOS hybrid switching amplitude modulator for edge polar transmitters," *IEEE J. Solid-State Circuits*, vol. 42, no. 12, pp. 2666–2676, Dec. 2007.

[4] C. Hsia, A. Zhu, J. J. Yan, P. Draxler, D. Kimball, S. Lanfranco, and P. M. Asbeck, "Digitally assisted dual-switch high-efficiency envelope amplifier for envelope-tracking base-station power amplifiers," *IEEE Trans. Microw. Theory Techn.*, vol. 59, no. 11, pp. 2943–2952, Nov. 2011.

[5] P. Y. Wu and P. K. T. Mok, "A two-phase switching hybrid supply modulator for RF power amplifier with 9% efficiency improvement," *IEEE J. Solid-State Circuits*, vol. 45, no. 12, pp. 2543–2556, Dec. 2010.

[6] D. Kim, D. Kang, J. Kim, Y. Cho, and B. Kim, "Wideband envelope tracking power amplifier for LTE application," in *IEEE Radio Freq. Integr. Circuits Symp.*, Jun. 2012, pp. 275–278.

[7] Y. Li, J. Lopez, P.-H. Wu, W. Hu, R. Wu, and D. Y. C. Lie, "Design of high efficiency monolithic power amplifier with envelope-tracking and transistor resizing for broadband wireless applications," *IEEE J. Solid-State Circuits*, vol. 47, no. 9, pp. 2007–2018, Sep. 2012.

[8] J. Choi, D. Kim, D. Kang, and B. Kim, "A new power management IC architecture for envelope tracking power amplifier," *IEEE Trans. Microw. Theory Techn.*, vol. 59, no. 7, pp. 1796–1802, Jul. 2011.

[9] W. Chu, B. Bakkalogle, and S. Kiaei, "A 10 MHz-bandwidth 2 mV-ripple PA-supply regulator for CDMA transmitters," in *IEEE Int. Solid-State Circuits Conf. Tech. Dig.*, Feb. 2008, pp. 448–449.

[10] J. Choi, D. Kim, D. Kang, and B. Kim, "A polar transmitter with CMOS programmable hysteretic-controlled hybrid switching supply modulator for multistandard applications," *IEEE Trans. Microw. Theory Techn.*, vol. 57, no. 7, pp. 1675–1686, Jul. 2009.

[11] D. Kim, D. Kang, J. Choi, J. Kim, Y. Cho, and B. Kim, "Optimization for envelope shaped operation of envelope tracking power amplifier," *IEEE Trans. Microw. Theory Techn.*, vol. 59, no. 7, pp. 1787–1795, Jul. 2011.

[12] J. Hoversten, S. Schafer, M. Roberg, M. Norris, D. Maksimovi, Z. Popovi, and B. Kim, "Codesign of PA, supply, and signal processing for linear supply-modulated RF transmitters," *IEEE Trans. Microw. Theory Techn.*, vol. 60, no. 6, pp. 2010–2020, Jun. 2012.

[13] Y. Li, J. Lopez, P.-H. Wu, W. Hu, R. Wu, and D. Y. C. Lie, "A SiGe envelope-tracking power amplifier with an integrated CMOS envelope modulator for Mobile WiMAX/3GPP LTE transmitters," *IEEE Trans. Microw. Theory Techn.*, vol. 59, no. 10, pp. 2525–2536, Oct. 2011.

[14] F. Wang, D. F. Kimball, D. Y. Lie, P. M. Asbeck, and L. E. Larson, "A monolithic high-efficiency 2.4-GHz 20-dBm SiGe BiCMOS envelope-tracking OFDM power amplifier," *IEEE J. Solid-State Circuits*, vol. 42, no. 12, pp. 2666–2676, Dec. 2007.

[15] M. Hassan, L. E. Larson, V. W. Leung, D. F. Kimball, and P. M. Asbeck, "A wideband CMOS/GaAs HBT envelope tracking power amplifier for 4G LTE mobile terminal applications," *IEEE Trans. Microw. Theory Techn.*, vol. 60, no. 5, pp. 1321–1330, May 2012.

[16] R. Shrestha, R. A. R. van der Zee, A. J. M. de Graauw, and B. Nauta, "A wideband supply modulator for 20 MHz RF bandwidth polar PAs in 65 nm CMOS," *IEEE J. Solid-State Circuits*, vol. 44, no. 4, pp. 1272–1280, Apr. 2009.

[17] D. Kang, B. Park, D. Kim, J. Kim, Y. Cho, and B. Kim, "Envelope-tracking CMOS power amplifier module for LTE applications," *IEEE Trans. Microw. Theory Techn.*, vol. 61, no. 10, pp. 3763–3773, Oct. 2013.

[18] J. Kim, D. Kim, Y. Cho, D. Kang, B. Park, and B. Kim, "Envelope-tracking two-stage power amplifier with dual-mode supply modulator for LTE applications," *IEEE Trans. Microw. Theory Techn.*, vol. 61, no. 1, pp. 543–552, Jan. 2013.

[19] "ACPM-5017 LTE Band12/17 (698–716 MHz) 3 $\times$ 3 mm power amplifier module," Avago Technol., San Jose, CA, USA, 2012. [Online]. Available: http://www.avagotech.com/docs/AV02-3006EN

[20] F. H. Raab, "Intermodulation distortion in Kahn-technique transmitters," *IEEE Trans. Microw. Theory Techn.*, vol. 44, no. 12, pp. 2273–2278, Dec. 1996.

[21] Y. Zhao, A. G. Metzger, P. J. Zampardi, M. Iwamoto, and P. M. Asbeck, "Linearity improvement of HBT-based Doherty power amplifiers based on a simple analytical model," *IEEE Trans. Microw. Theory Techn.*, vol. 54, no. 12, pp. 4479–4488, Dec. 2006.

[22] D. Kang, D. Yu, K. Min, K. Han, J. Choi, D. Kim, B. Jin, M. Jun, and B. Kim, "A highly efficient and linear class-AB/F power amplifier for multimode operation," *IEEE Trans. Microw. Theory Techn.*, vol. 56, no. 1, pp. 77–87, Jan. 2008.

[23] C. Fager, J. C. Pedro, N. B. Carvalho, H. Zirath, F. Fortes, and M. J. Rosário, "A comprehensive analysis of IMD behavior in RF CMOS power amplifiers," *IEEE J. Solid-State Circuits*, vol. 39, no. 1, pp. 24–34, Jan. 2004.

[24] E. Malaver, J. A. García, A. Tazón, and A. Mediavilla, "Characterizing the linearity sweet-spot evolution in FET devices," in *Proc. 11th GaAs Symp.*, Munich, Germany, Oct. 2003.

[25] R. Sperlich, Y. Park, G. Copeland, and J. S. Kenney, "Power amplifier linearization with digital pre-distortion and crest factor reduction," in *IEEE MTT-S Int. Microw. Symp. Dig.*, Fort Worth, TX, USA, Jun. 2004, pp. 669–672.

[26] O. Degani, F. Cossoy, S. Shahaf, E. Cohen, V. Kravtsov, O. Sendik, D. Chowdhury, C. D. Hull, and S. Ravid, "A 90-nm CMOS power amplifier for 802.16e (WiMAX) applications," *IEEE Trans. Microw. Theory Techn.*, vol. 58, no. 5, pp. 1431–1437, May 2010.

[27] *3rd Generation Partnership Project; Technical Specification Group Radio Access Network; Evolved Universal Terrestrial Radio Access (E-UTRA); User Equipment (UE) Radio Transmission and Reception (Release 8)*, 3GPP, 2009.

Jooseung Kim (S'12) received the B.S. degree in electrical engineering from the Pohang University of Science and Technology (POSTECH), Pohang, Korea, in 2010, and is currently working toward the Ph.D. degree in electrical engineering at POSTECH.

His research interests are CMOS RF circuits for wireless communications, with a special focus on highly efficient and linear RF transmitter design.

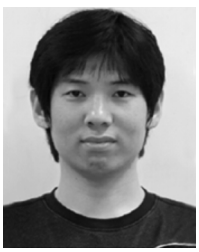

Dongsu Kim received the B.S. and Ph.D. degrees in electronic and electrical engineering from the Pohang University of Science and Technology (POSTECH), Pohang, Korea in 2007, and 2013, respectively.

He is currently with Samsung Electronics, Suwon-si, Gyeonggi, Korea. His research interests are CMOS RF circuits for wireless communications with a special focus on highly efficient and linear RF transmitter design.

Yunsung Cho (S'12) received the B.S. degree in electrical engineering from Hanyang University, Ansan, Korea, in 2010, and is currently working toward the Ph.D. degree in electrical engineering at the Pohang University of Science and Technology (POSTECH), Pohang, Korea.

His main interests are RF circuits for wireless communications, especially highly efficient and linear RF transmitters and RF PA design.

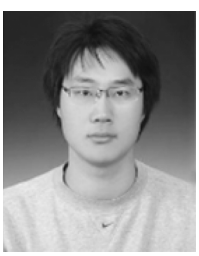

Daehyun Kang received the B.S. degree in electronic and electrical engineering from Kyungpook National University, Daegu, Korea, in 2006, and the Ph.D. degree in electrical engineering from POSTECH, Pohang, Korea, in 2012. His doctoral research focused on RF circuits for wireless communications, especially efficient RF TX and RF PA design.

In 2011, he was an Intern with RF Micro Devices, Cedar Rapids, IA, USA, where he designed balanced and single-ended LTE PAs. Since 2012, he has been with the Broadcom Corporation, Matawan, NJ, USA, where he is involved with mobile system designs. His current research interests include advanced transmit/receive (TX/RX) architectures for mobile communications.

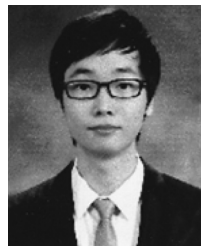

Byungjoon Park received the B.S. degree in electrical engineering from Hanyang University, Seoul, Korea, in 2010, and is currently working toward the Ph.D. degree in electrical engieering from the Pohang University of Science and Technology (POSTECH), Pohang, Korea.

His main interests are RF circuits for wireless communications, especially highly efficient and linear RF transmitters and RF PA design.

Kyunghoon Moon (S'13) received the B.S. degree in electrical engineering from Hanyang University, Ansan, Korea, in 2012, and is currently working toward the Ph.D. degree in electrical engineering at the Pohang University of Science and Technology (POSTECH), Pohang, Korea.

His main interests are RF circuits for wireless communications, especially highly efficient and linear RF transmitters and RF PA design.

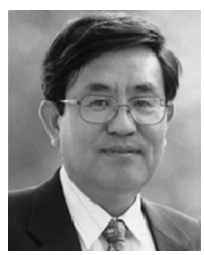

Bumman Kim (M'78–SM'97–F'07) received the Ph.D. degree in electrical engineering from Carnegie Mellon University, Pittsburgh, PA, USA, in 1979.

From 1978 to 1981, he was engaged in fiber-optic network component research with GTE Laboratories Inc. In 1981, he joined the Central Research Laboratories, Texas Instruments Incorporated, where he was involved in the development of GaAs power field-effect transistors (FETs) and monolithic microwave integrated circuits (MMICs). He has developed a large-signal model of a power FET, dual-gate FETs for gain control, high-power distributed amplifiers, and various millimeter-wave MMICs. In 1989, he joined the Pohang University of Science and Technology (POSTECH), Pohang, Korea, where he is a POSTECH Fellow and a Namko Professor with the Department of Electrical Engineering and Division of Information Technology Convergence Engineering (ITCE), and Director of the Microwave Application Research Center. He is involved in device and circuit technology for RF integrated circuits (RFICs) and PAs. He has authored over 400 technical papers.

Prof. Kim is a member of the Korean Academy of Science and Technology and the National Academy of Engineering of Korea. He was an associate editor for the IEEE TRANSACTIONS ON MICROWAVE THEORY AND TECHNIQUES. He was a Distinguished Lecturer of the IEEE Microwave Theory and Techniques Society (IEEE MTT-S) and an Administrative Committee (AdCom) member.